J. Condensed Matter Nucl. Sci. 15 (2015) 203–230

Research Article

Possibility of Tachyon Monopoles Detected in Photographic Emulsions

Keith A. Fredericks*

Restframe Labs, W. Lafayette, IN 47906, USA

Abstract

Low-energy nuclear reaction experiments using photographic emulsions, including those by Urutskoev, et.al, Ivoilov, and others have shown unique particle tracks. Analysis of a sample population of these types of tracks suggests detection of magnetically charged particles with faster-than-light velocities. Particle kinetic energy was estimated from energy deposition and momentum was estimated from track curvature in magnetic fields. Measured values were plotted on a kinetic energy versus momentum graph and were found to fall in the $v > c$ region. Track curvature was found to be parabolic, which is a signature for monopoles. Using the classical theory of tachyons, the plane of parabolic curvature suggests electrically charged tachyons detected as slower-than-light monopoles. Preliminary lower limits for particle mass are found. Further study is suggested to broaden this search.
 ISSN 2227-3123

Keywords: Detection, Mass Estimate, Monopoles, Parabolic curvature, Photographic emulsion, Superluminal, Tachyons

1. Introduction

A recent preliminary analysis of unique particle tracks [1] is consistent with the possible detection of tachyons (faster-than-light particles) as shown by four signatures

(1) Kinetic energy vs. momentum values are consistent with $v > c$ particles
(2) A superluminal Lorentz transformation (SLT) rectifies particle mass and velocity confirming the particle as a tachyon
(3) Parabolic curvature in applied magnetic fields is unique to monopoles, but the observed plane of curvature is incorrect
(4) An SLT rectifies the orientation of the Lorentz force acting on the particle confirming the particle as a tachyon (monopole)

This result is testable by repeating one or more of the six experiments yielding particle tracks (in Section 2) in a perpendicular applied magnetic field followed by analysis of the parabolic curvature, kinetic energy and momentum

*E-mail: keith@restframe.com

 ISSN 2227-3123

of the particle tracks. Certain additional particle properties are considered and seen to fit within the framework of the classical theory of tachyons. As these types of particle tracks have been observed in experiments associated with Low Energy Nuclear Reactions (LENR), it is possible that these particles play a role in the as yet unknown mechanism of these reactions.

1.1. Background

A unique collection particle track effects has been observed in a variety of studies [1–13] since 1979. The same track effects have been observed in diverse experiments including bombardment by low-energy ions in glow discharge plasma processes [10,11], electric explosion of metallic wires and thin foils [2,3,6], low-energy discharges in water [4,5], electrolysis with Pd cathodes in H_2O [12,13], the search for monopoles of solar origin at the north pole [7], the supercompression of solid targets using electron beams [8,9], and exposure to human hands [1]. All experiments cited here recorded particle tracks using photographic emulsions except [8,9], which recorded tracks with MDS (metal–dielectric–semiconductor).

Our experiments [1], from 1979 observed track effects primarily under conditions where human fingertips were *exposed* to photographic emulsions. The use of amplified photographic emulsions in these experiments significantly enhanced the sensitivity to the track effects and facilitated the recording of a number of important effects not observed in other experiments and led to the largest and most comprehensive set of particle tracks with over 200 exposures and well over 1000 tracks.

The data generated in these experiments replicates very closely virtually all track effects observed in [2–11] and shares properties with [12,13]. The tracks exhibit certain properties in photographic emulsions and other materials and are characterized as to their curvature in magnetic fields, length, width, periodic structure, random motion, correlation, splitting, and vertex structure. These properties considered together begin to form a picture of a particle that creates unique tracks in photographic emulsions and other materials and that must represent a new type of elementary particle.

The paper is organized as follows:

- Section 2: Review of Studies
- Section 3: Particle Properties
- Section 4: ζ-Correction
- Section 5: Momentum
- Section 6: Energy Loss
- Section 7: Superluminal Lorentz Transformation
- Section 8: Discussion
- Section 9: Conclusion

2. Review of Studies

These unique track observations are shared between several studies. Most of these studies [2–6,8–13] fall into the category of LENR or CMNS (Condensed Matter Nuclear Science) [14–16]. Data from Fredericks [1] and Bardout [7] do not involve electrical discharges, but show the same tracks. The identity between the results of these two types of experiments is established [1] and it is possible that the particles creating these tracks are involved with LENR either as a catalyst or a by-product.

The amplification of photographic detectors used in Fredericks [1] yielded the most extensive collection of track types, including those shown in each of the LENR studies and therefore represents a super-set of all tracks. Track types were categorized and related to particle properties.

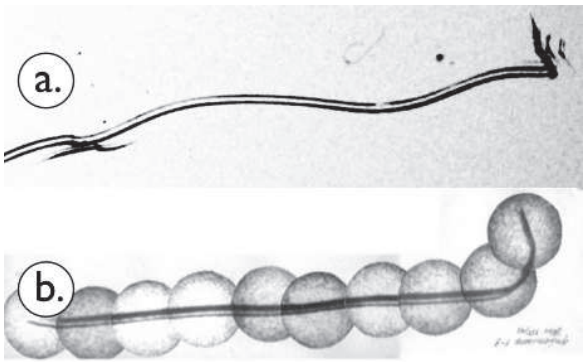

Figure 1. (a) Fredericks track in Polychrome Litho film. Compare with tracks in Section 3.10 and Fig. 6 in Priem et al. [6] (b) Urutskoev track. "Typical track" of Urutskoev and co-workers.

Each of the studies is briefly described and representative particle track images from each study are compared with matching images from Fredericks [1].

2.1. Urutskoev and co-workers

Urutskoev and co-workers [2] observed the transmutation of elements in a series of experiments using exploding wires and foils in liquids in reaction vessels. Fluoroscopic, radiographic and nuclear track emulsions were arranged at a distance from the reaction vessel or from samples of reaction by-products and were exposed for certain periods. Magnetic fields of $B \sim 20$ G were applied at the reaction site and $B \sim 1.2$ kG were applied at the detector.

They observed "strange radiation" on the emulsions and reported a number of track types, including *comets*, *spirals*, *gratings* and *caterpillar traces*.

Other properties observed were twin tracks, large-angle deflections, vertexes and track width that varied with distance from the source. Urutskoev and co-workers in collaboration with Georges Lochak forwarded a theory of *Lochak monopoles* [17] as a possible explanation of the particle track observations.

2.2. Ivoilov

Ivoilov [4] extended the work of Urutskoev and co-workers using low-energy discharges with carbon electrodes in liquids and excitation of beta-decay products in magnetic fields. The experimental setup was surrounded at a distance of 10–15 cm from the *source of the radiation*. Double-sided X-ray film was exposed in a perpendicular applied magnetic field for 3–10 min. during the discharge. Ivoilov observed long tracks up to 10 mm with regular periodic structure, large-angle deflections and curvature and states that the results were *completely identical* to those of Urutskoev and co-workers.

Ivoilov forwarded the important idea of internal reflection between the film base/gelatin and gelatin/air interfaces as responsible for the very long track lengths observed. Ivoilov was also the first to call attention to correlated tracks exhibiting rotational symmetry that Lochak called *chiral symmetry*. These types of tracks are shown in Figs. 2 and 17 and related to Figs. 24,23 and 19.

A connection is made between chiral tracks and north and south monopoles, but this is heuristic as there is no explanation of exactly *why* north and south monopoles would appear in opposite sides of ~ 10 μm double-sided (presumably commercial) X-ray films (on polyester base) using "reflectors" of Al, glass, Ge or Si behind the film.

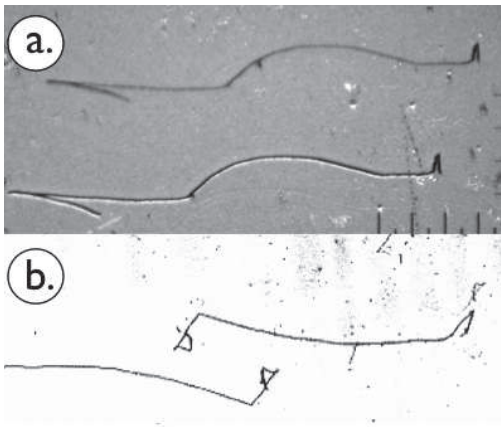

Figure 2. (a) Fredericks tracks. Correlated tracks in Kodak Kodalith type III film. Tracks are copies instead of mirror images or chirally transformed. (b) Iviolov "chiral" tracks. Multiple correlated tracks can be seen in the original image. The chirally transformed track is explained in the Ivoilov analysis as a reflected track which is recorded on the bottom emulsion facing an aluminum plate with polyester base material sandwiched between the two emulsion layers. Unspecified type of double-sided X-ray emulsion.

2.3. Rodionov and Savvatimova

Rodionov and Savvatimova [10] reviewed experiments where particle tracks were observed on photographic emulsions and surfaces of metal electrodes. They generated images in emulsions surrounding glow discharges in plasma and recorded track images on metal electrodes from the reaction vessel.

The tracks have widths usually about 10 μm, lengths of millimeters and more, repeated patterns *like tire treads or necklaces, continuous lines, groups of lines and parallel lines*.

Several images are shown of tracks in Pd cathodes and in Kodak BioMax (autoradiographic emulsion), RT-2 X-ray, and nuclear track emulsions. These images show large-angle deflections or vertexes where two tracks co-terminate, and tracks with regular periodic structure, some of which are labeled as spirals. A regular periodic structure *parabolic* track on a Pd cathode from this study is analyzed in our earlier paper [1].

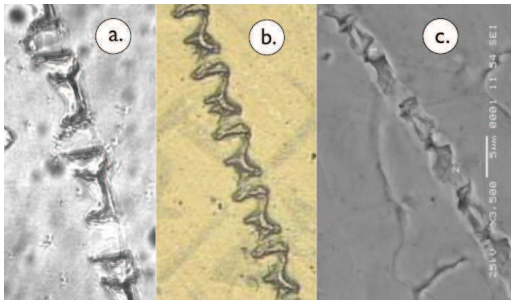

Figure 3. (a) Fredericks track on Polychrome litho film. (b) Rodinov and Savvatimova periodic structure track on nuclear emulsion. Note similarity to Fredericks track where "hourglass" structures are separated by flat structures. (c) Rodinov and Savvatimova periodic structure track on Pd cathode from scanning electron microscope.

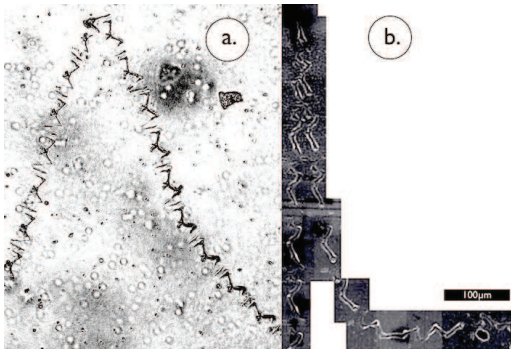

Figure 4. (a) Fredericks track (b) Adamenko and Vysotskii track evaporated in MDS showing parabolic curvature. Detail of track using high magnification.

2.4. Adamenko and Vysotskii

Adamenko and Vysotskiiadamenko.1,adamenko.2 use a method of supercompression of solids with a high-current vacuum tube diode leading to the transformation of nuclei. In these experiments, the authors find tracks on the surfaces of MDS (Metal Dielectric Semiconductor Al–SiO_2–Si sandwich) targets. The tracks created in the MDS are said to be *analogous* to the Urutskoev tracks in photographic emulsions.

Total energy required for the formation of the track was calculated to be $\approx -10^6$ GeV/cm. Particle mass is estimated based on the assumption of magnetic charge to be $\approx 10^{-23}$ g ($\approx$ 560 GeV). The authors suggest that the particle may fit within the framework of a magnetic monopole and in particular the Lochak monopole.lochak.equation

The particle track shown exhibits either a very large-angle deflection or the co-termination of two tracks. One half of the track shows a great deal of smooth curvature (much of which is parabolic). The very good micrographs give an unprecedented view of the almost perfectly correlated periodic structure of each part of the track leading up to the large-angle deflection.

2.5. Priem et al.

Priem et al. [6,18] replicated the experiments of Urutskoev [2] and found good agreement with their results related to both the by-products of the explosion of wires and the subsequent recording of particle tracks similar to

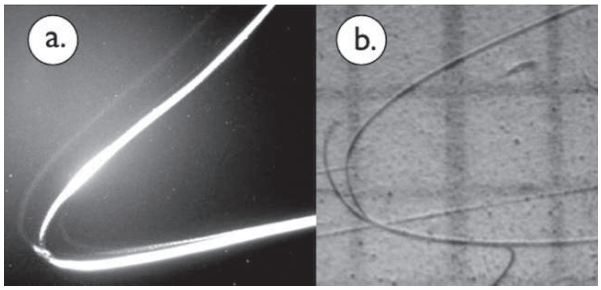

Figure 5. (a) Fredericks track. (b) Priem et al. track. On both tracks, parabolic curvature and splitting are seen.

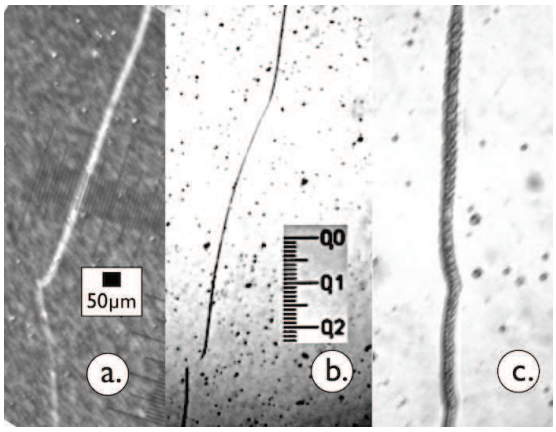

Figure 6. Tracks a and b are classic 2-tailed vertexes with convex curvature. The curved part of track b is difficult to see, but appears to be parabolic. Track a was measured to be parabolic. (a) Fredericks track in Kodak Kodalith type III film. (b) Bardout et al. track in Kodak Industrex MX125 (double-sided) film. (c) Related Lochak "laboratory" tracklochak.web showing regular periodic structure.

Urutskoev et al. Of primary interest are photographic observations of *parabolic tracks* (not noted as such in their work), tracks with regular periodic structure as in Urutskoev et al. [2] and tracks with random or "irregular" structure. Each of these track types correspond to a specific track type in our study.

2.6. Bardout et al.

Bardout et al. [7] reported on photographic results from an expedition to the North Pole where Lochak's prediction regarding the detection of monopoles traveling from the sun to the earth was tested. Three tracks, exposed on Kodak Industrex MX125, are shown. The authors note that the tracks are similar to those detected in Urutskoev et al. Large-angle deflections are seen in very long tracks with regular periodic [a] [19] internal structure. Tracks a and b in Fig. 6 are consistent with *two-tailed vertexes* shown in Section 3.11.

2.7. Matsumoto

Matsumoto [12,13] performed electrolysis experiments in glass cells wit platinum anodes and palladium cathodes in a solution of ordinary H_2O with 0.5 M K_2CO_3. The experiments were instrumented with 50 and 100 μm MA-7B Fuji Film nuclear emulsions. Matsumoto generated a series of images apparently distinct from other studies considered here, but similarities to our group of studies is seen in track structure and correlation.

The track structure in the *star* image in Fig. 7 of Matsumoto [13] shows distinct circular periodic structure similar to images of Fredericks [1]. In Matsumoto's *ring* images, nearly perfectly circular ring images are shown. Rotational symmetry is exhibited in images exposed on adjacent facing double-sided plates in Figs. 19 and 20. This type of symmetry appears to be related to observations by Ivoilov [4,5] and Fredericks [1]. Matsumoto attributed his unique images to ball lightning and microscopic black and white holes.

[a] G. Lochak, personal communication.

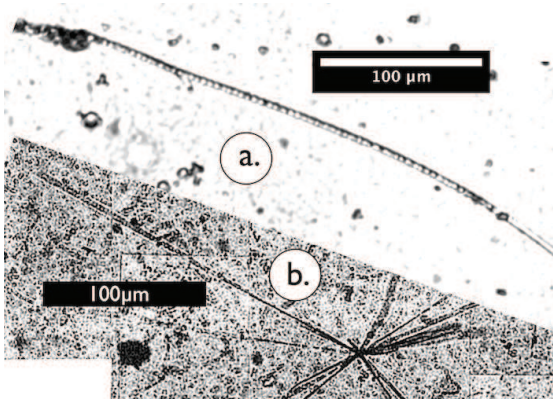

Figure 7. Both tracks exhibit regular periodic "circles" in tracks. (a) Fredericks track (b) Matsumoto *star* in Fujifilm MA-7B nuclear emulsion.

2.8. Fredericks

These experiments exposed human fingertips to emulsions for 2–30 min and many experiments were carried out with an applied magnetic field perpendicular to the plane of the emulsion. The effect was shown to occur independently of a dielectric isolator included between the fingertips and the photographic emulsion surface [1]. Film type, amplification and development were analyzed. The tracks were observed on six different film types using two different types of photographic development [1].

A special photographic amplification technique was employed, making possible a higher level of photographic sensitivity specifically for line and dot images, greatly enhancing track visibility [1].

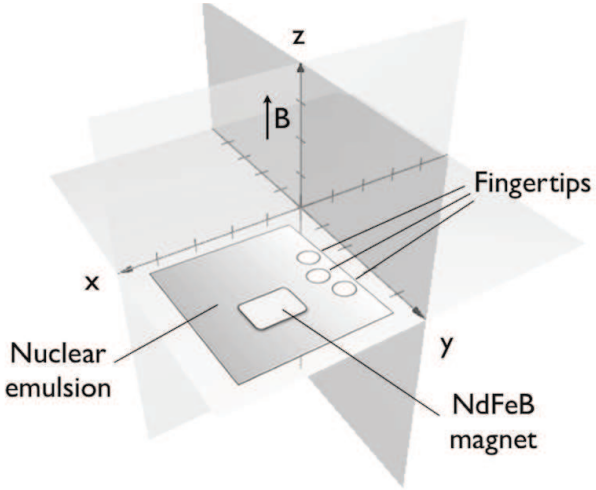

Figure 8. Experimental setup of Fredericks showing M3, a neodymium permanent magnet.

Track observations [1] included parabolic curvature in applied magnetic fields, strong correlation, regular periodic structure, numerous large-angle deflections, random motion, and correlated random motion.

2.9. Commentary

Bardout [7] and particularly Fredericks [1] stand out from the other studies due to the absence of any electrical explosions, discharges, their by-products or applied electric fields, which constitute in [2–6, 8–13] the assumed source (or catalyst) of the phenomena. It is remarkable with these differences in exposure conditions that Fredericks duplicates virtually all observed track types. The only track types specifically *not observed* were the Ivoilov [4,5] "chirals" and the Matsumoto [13] "rings." A relationship between all of the tracks in the present study is clearly established indicating a commonality of exposure, the mechanism of which is not clear. The studies in [2–9] and analyses by Lochaklochak.equation,lochak.lenr envision the *Lochak* monopole as responsible for these particle tracks, but without solid support for this hypothesis.

3. Particle Properties

3.1. Image formation

In the following we refer to the state of photographic development of the track image and the central track image in tracks with a border effect. Track images are formed on photographic film in one of three ways:

(1) *Type 1*. Excitation of of the AgBr crystals via either ionization or light causing track images via developed AgBr crystals. This is referred to as "positive" or "normal exposure." This type of track image is seen on the emulsion as a dark line on a lighter background.
(2) *Type 2*. Bleaching of the AgBr crystals via an unknown mechanism causing track images via the absence of developed crystals. This is referred to as "reversal" or "bleaching." This type of track image is seen on the emulsion as a white line on a darker background.
(3) *Type 3*. Direct action on the gelatin and possibly the plastic base producing track images via the removal and/or deformation of plastic or gelatin. This is referred to as "evaporated." This category of track images can be clear, but visible due to the refraction of light and can also be accompanied by developed silver in the repeating patterns.

Type 3 image formation is unusual in the area of photographic science and indicates a non-standard action occurring in the emulsion. Regular periodic structures are seen on photographic emulsions, Pd cathodes, and MDS semiconductor surfaces. A connection may exist between the elevated energies required to expose tracks on metal or semiconductor surfaces and "evaporated" track images in the plastic base of emulsions.

3.2. Lines and dots

The tracks appear as dots and lines. Dots indicate angles of incidence of particles more perpendicular to the plane of the emulsion. Lines indicate angles of incidence more parallel to the plane of the emulsion. Dots appear in various sizes, generally corresponding to track cross section dimensions. Some dots are substantially larger and some are "smeared." Some of these smeared tracks correspond to the *comet* tracks of Urutskoev et al. (see Fig. 16a. in [2]).

3.3. Track width

Our track width measurements can be compared with studies by Urutskoev [2] and Iviolov [4] where 5–30 μm track widths were measured. They found that track width decreased as detector distance from the source was increased.

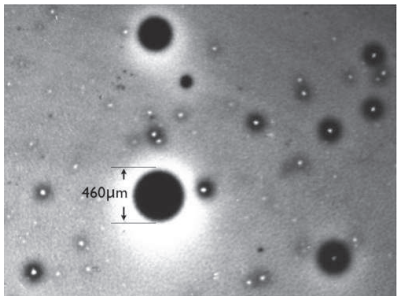

Figure 9. Micrograph at 25× of dots. Note the internal structure of all-black dots and dots with white centers. Kodak type NTB3 10 μm emulsion.

Track width has been measured to have a range of at least 5–110 μm (horizontal) and 5–460 μm (vertical).

In our studies, tracks have been observed with and without image amplification. In exposures with amplification, the inner track is surrounded by an edge, fringe or halo effect on both sides of the track, which increases the visibility of these images [1].

3.4. Track length

Figure 10 shows a 69 mm track. It is not clear if tracks have begun or ended in the emulsion. It is not immediately clear in what direction particles producing these tracks traveled although it may be possible to find track direction and charge by analyzing correlated pairs and groups of tracks in magnetic fields, which is the subject of future work.

There is tapering on both ends of the 69 mm track. Since a specific type of tapering is expected for monopoles [22], it may be of interest to analyze this tapering in detail.

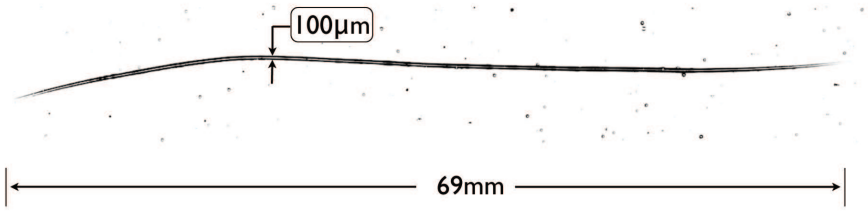

Figure 10. *69 mm* track in Kodak NTB3 type emulsion. The track width average is 91 μm.

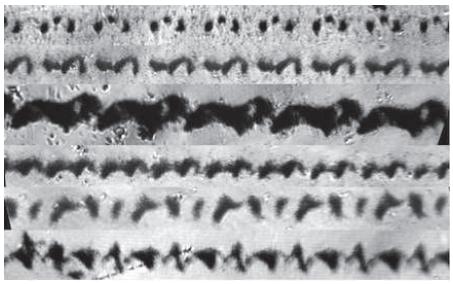

Figure 11. Different types of positive regular periodic structure tracks in Polychrome Litho film, no pre-exposure, developed with constant agitation.

3.5. Regular periodic structure

Under magnification, tracks with regular periodic structure are seen. Certain tracks have a completely periodic structure whereas other tracks change in mid-track from wholly saturated tracks to periodic tracks (and possibly back to wholly saturated). Some totally saturated tracks show underlying periodic structure suggesting an intrinsic periodic track structure.

Under low magnification, regular periodic structure tracks bear a closer resemblance to conventional charged particle tracks. These tracks however possess a much greater track length than conventional particles *and* a regular periodic structure as opposed to the random nature [23] of grain patterns in conventional nuclear track studies. Under higher magnification, regular periodic structure tracks show specific repeated patterns. Others have called these patterns "beaded necklaces" and "caterpillars." The regular periodic structure is suggestive of helical trajectories or trajectories with some type of periodic, or possibly chaotic, spin component.

3.6. Reversed tracks

Tracks can appear as either exposure (black, positive) or bleaching (white, reversed) The percentage of positive tracks versus reversed tracks has not been measured.

"Reversed" tracks appear to have formed due to a process that tears down or bleaches the latent image rather than

Figure 12. Different types of "evaporated" regular periodic structure tracks in Polychrome Litho film, no pre-exposure, developed with constant agitation.

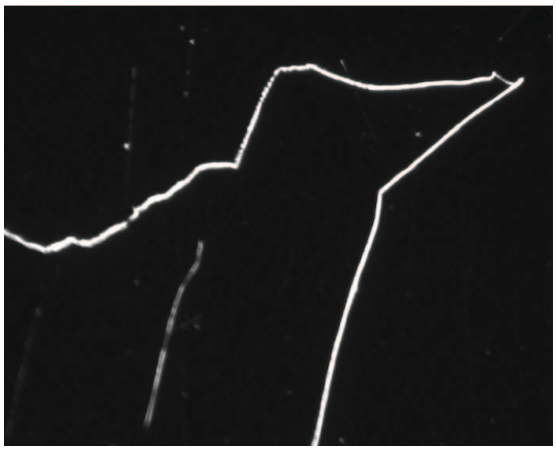

Figure 13. Photomicrograph of single track from Fig. 24, "Vector Swarm."

a process that creates a developable latent image. Other examples of such tracks are shown in Figs. 14 and 24. In photographic processes where this type of bleaching occurs, the mechanism is probably a reversal effect caused by rehalogenation of the latent image. When both positive and reversed tracks are observed on the same exposure, the different tracks may be due to particles with different energy levels.

3.7. Track curvature

Photographic nuclear track studies commonly require magnetic fields at least 100 times greater than those used in bubble chambers to produce measurable curvature in a photographic emulsion. In fact photographic emulsions are generally not used to observe charged particle curvature in applied magnetic fields. The observations considered here resemble tracks in bubble chambers more than tracks in photographic emulsions. This indicates highly penetrating particles and non-standard track exposure mechanisms.

In virtually all exposures where a perpendicular magnetic field was applied with respect to the plane of the emulsion, track curvature is observed to be *exactly parabolic*. See also Figs.23,26 and 28. Curve fitting in Section 5.1 shows parabolic curvature with high confidence. Particle momentum is estimated from track curvature in Section 5.2.

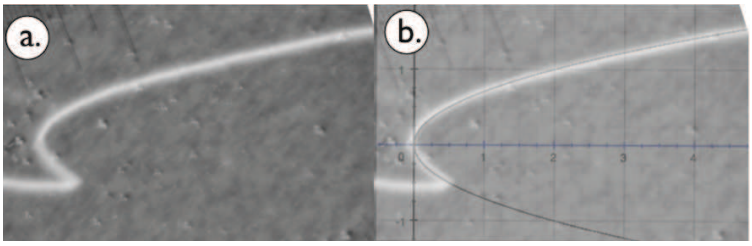

Figure 14. *Hook*, Curved track in Kodalith type III film. Applied magnetic field of permanent magnet M3. (a) Raw track. (b) Graph of parabola $x = y^2$ overlaid on track.

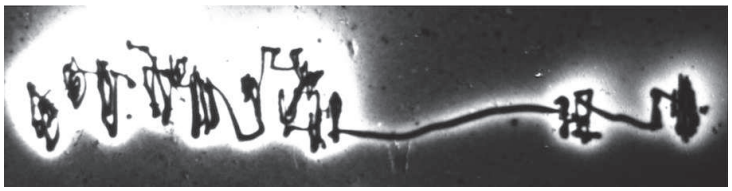

Figure 15. *squiggle2* Random motion type tracks in Kodak NTB3 10 μ nuclear emulsion. Extreme large angle deflections and continuous smooth curvature are shown. Minimum track width = 10 μm, track linear measure = 4.3mm.

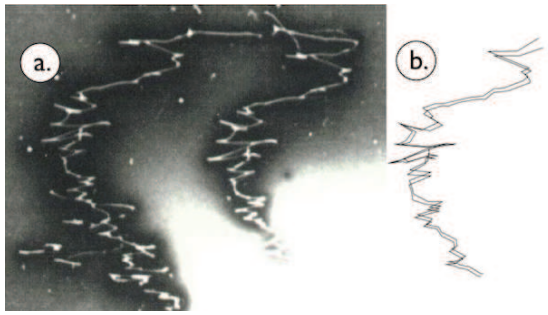

Figure 16. (a) Correlated random motion trajectories. Kodak 10 μm NTB3 emulsion. (b) Using a graphics editor, the tracks were traced from the original. The tracks when superimposed upon each other reveal very similar though not quite identical structure.

3.8. Random motion tracks

Large-angle deflections are very rare in photographic emulsions.powell In these tracks, with linear measure up to ~ 5 mm, large-angle deflections are numerous.

3.9. Correlated tracks

Correlated trajectories and correlated random motion trajectories have not been seen in any standard photographic nuclear track studies done to date.

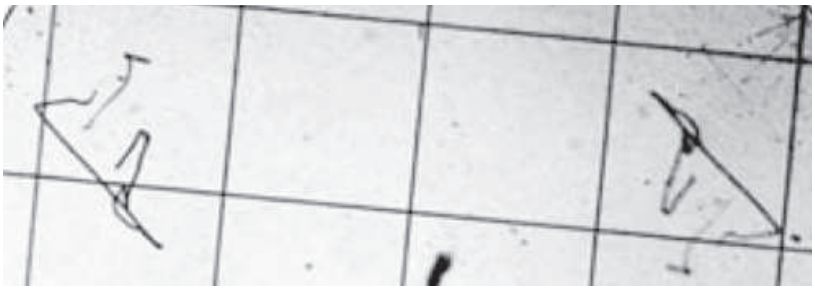

Figure 17. Ivoilov “chiral”" tracks in original orientation

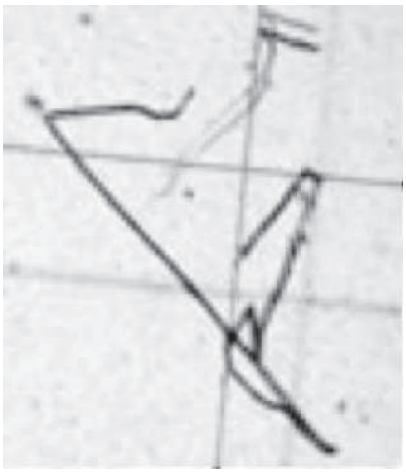

Figure 18. Ivoilov "chiral" tracks where right track was flipped horizontally and vertically and overlaid on left track. Note correspondence on main track and misalignment on other tracks. Compare with Fredericks tracks in Fig. 16 where two correlated tracks are overlaid.

In images shown by Ivoilov [4] and analyzed by Lochak [17], tracks exhibit rotational symmetry. Ivoilov used glass, Al, and monocrystalline Ge and Si as *reflectors* behind double-sided X-ray film. These images can be overlaid with only minor differences between them, see Fig. 18.

In conjunction with Georges Lochak, Ivoilov proposed that the observations were due to the *Lochak* monopole [17] and further that the pairs of detected particles were *chirally symmetric*. Figure 19 in Matsumoto [13] has characteristics of Ivoilov correlations in that similar images are captured on two pieces of film, but the correlation may

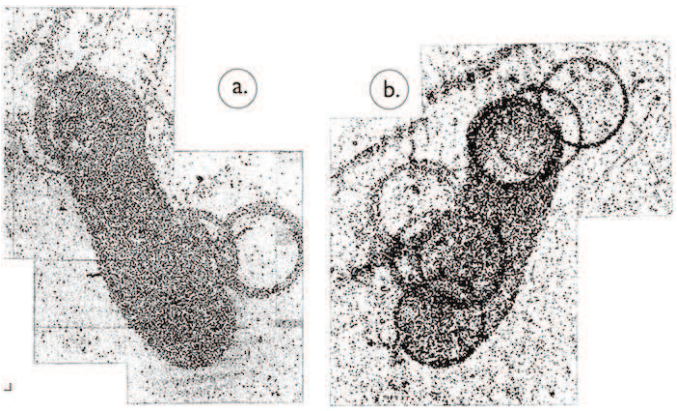

Figure 19. Matsumoto correlated tracks as presented in original publication.

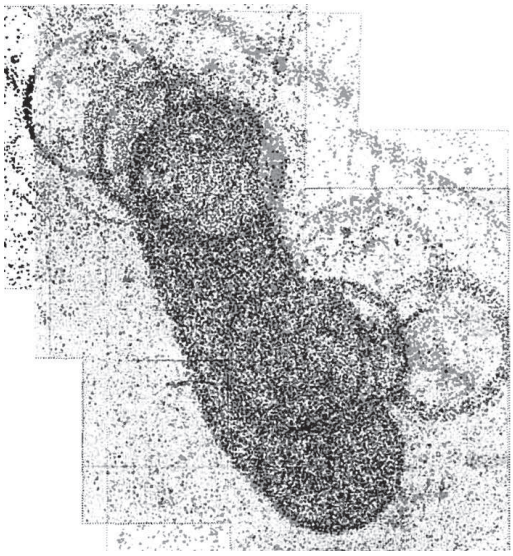

Figure 20. Matsumoto correlated tracks overlaid. The shape of the image and certain ring positions correspond.

be more closely related to translational type symmetry as in the Fredericks images rather than a rotational symmetry as in studies of Ivoilov.

Correlation of these particle tracks is the rule and not the exception. Particles often travel in pairs or groups, shown in the analysis as tracks with a very high degree of correlation, even in the case of extremely complex trajectories. Particles found to be correlated throughout each of their trajectories appear to be connected. It is tempting to view this condition as a correlated particle experiment with the correlated tracks a visualization of entanglement.

In addition to observations of tracks in pairs, tracks in groups are also seen. If a permanent magnet is used in the experiment, it is likely that correlated groups of tracks will appear. Effects due to a non-uniform applied magnetic field are seen in Figs. 21–24.

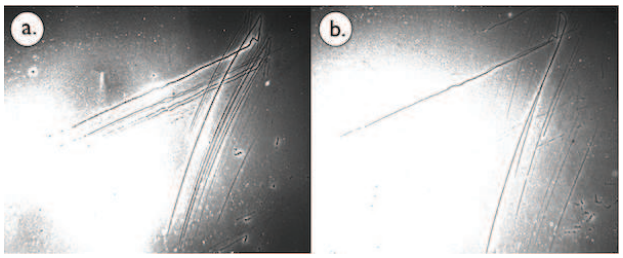

Figure 21. *Bobby pins* raw tracks in Kodak NTB3 10 μm emulsion. Tracks a and b are separated by a few millimeters on the film. Tracks have many of the same features, except that track a has a loop, i.e., the track crosses itself whereas track b does not. These tracks are correlated in position extremely well until the critical region (segment 19 in Fig. 22) when track a has a large angle deflection to the left and track b has a corresponding smoothly curving deflection to the right. Susceptibility to magnetic deflection appears to be overwhelming or twisting the correlation.

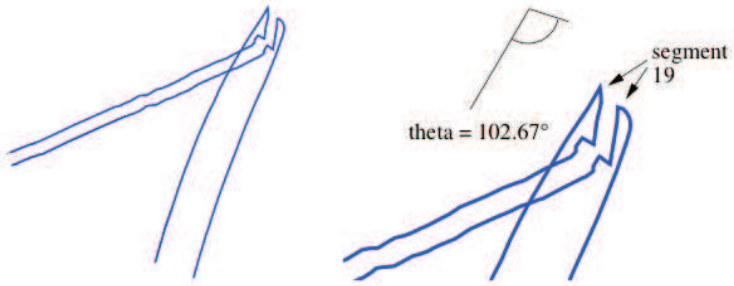

Figure 22. Digitized tracks from Fig. fig:bobby-pins

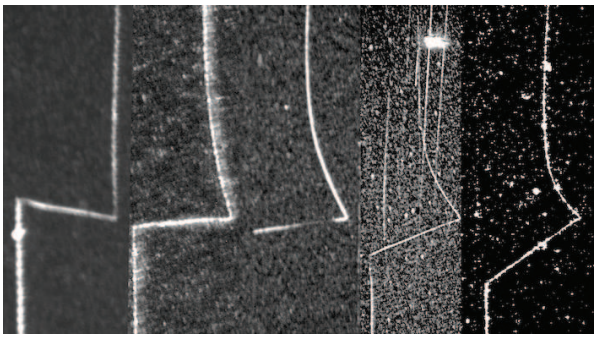

Figure 23. Progressive curvature seen in a correlated group of tracks from the same exposure.

Figure 24. *Vector Swarm* Group correlation of tracks including random motion components. These tracks do not line up when overlaid. They change form with location, apparently due to relative position in the applied non-uniform magnetic field. A large number of the tracks in this exposure are correlated. A measure of corresponding line segments of matching groups of tracks reveals a macroscopic "central force," which will be the subject of future work.

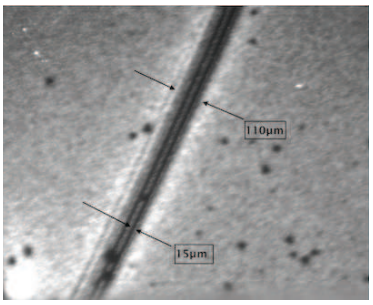

Figure 25. *Sub Tracks Detail* Micrograph at 45x magnification showing sub-track structure of the track bundle.

Turning to Fig. 24, a very interesting region of track exposures was found. As with certain of the previous exposures, correlation of track images was seen. But instead of an entire group of carbon copies, we see a field of complex track structures with the same set of line segments, but each set of line segments has its own unique individual geometric transformation.

The group of track exposures appears to be subject to a *geometric center* related to magnetic field strength. This may reconcile observations of rotational and translational symmetry as translations with respect to electromagnetic fields. Figure 24 shows conclusive evidence of a real particle effect and what can only be a group of "identical" correlated particles going through a series of quantum transitions in a non-uniform magnetic field.

3.10. Track bundles

Tracks with internal structure and large measured widths are observed to apparently split in places. In light of this, it is postulated that these particles can travel in bundles and that they can undergo various transitions such as splitting into correlated twins or swarms. Lower energy particles may be the result of the splitting of the higher energy bundle.

The result of Urutskoev et al. where they observed larger tracks closer to the source and smaller tracks at a further distance from the source may indicate that decay and splitting occurs for these particles over a one meter distance reducing a 30–5 μm track. It is noted that Urutskoev et al. [2] mentioned the idea that certain of the "ink blot" style tracks may be modeled as particle "clusters." If the particles are traveling in bundles, a computation of particle energy or mass needs correction with respect to the base particle mass. One way to do this correction is shown in Section 4.

3.11. Vertexes

In the set of all tracks, several types of vertexes are observed, but one type of vertex stands out. This is the two-tailed vertex. Of particular interest is where one of the track segments is curved and the other is straight. These structures are either singular or infrequent in long tracks. They very often have similar features and are seen in either *concave* or *convex* configurations. These types of vertexes have been observed also in other studies [2–5,7–11]. Eighteen of these *two-tailed* tracks were selected for track curvature and energy deposition measurements and are the subject of analysis in Sections 5.2–7.

4. ζ-Correction

Based on the observation that the particles are traveling in bundles, a correction factor is created

$$\zeta = \frac{w}{w_0}, \tag{1}$$

where w_0 is the actual smallest track width measured for a single particle and w is the measured track width of a given track. For this study $w_0 = 5\ \mu m$. ζ was measured and utilized in computations for a number of tracks including the 18 sample tracks [1].

5. Momentum

Tracks appear in photographic emulsions much like they would be expected to appear in a bubble chamber, often with long (>cm) track lengths and smooth curvature in magnetic fields, so it is straightforward to make track curvature measurements on the tracks as is done for bubble chamber photographs. Initially it was thought that the curvature of these tracks was circular. (This error was also made in [6].) Using an overlay of a $y = x^2$ parabola, the tracks can be seen visually in Figs. 14,26 and 28 to be parabolic. Fitting curves to the 18 tracks, in Section 5.1, confirms this with excellent fits over the sample of tracks.

5.1. Parabolic curvature

In Fig. 27, parabolic curvature can occur for

(1) electrically charged particles in an applied *electric* field,
(2) magnetically charged particles in an applied magnetic field.

There is no applied electric field in any of our exposures and the curvature is observed in the x, y plane instead of *the* x, z *plane* where parabolic curvature is expected for a particle with magnetic charge.

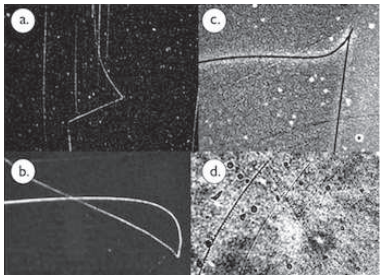

Figure 26. (a) One of a series of tracks with progressive curvature. Concave reversed track. Exact fit to parabola. (b) The classic vertex form. Convex positive track. Exact fit to parabola. (c) The concave form of the vertex. Reversed track. Exact fit to parabola. (d) Small convex form track using 400× magnification. Evaporated track. Exact fit to parabola.

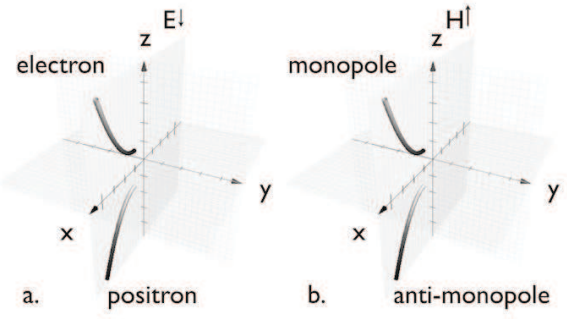

Figure 27. (a) An electric field, E is applied along the z-axis in the -z direction. Due to the E field, electrons curve upward and positrons curve downward in a parabola in the x, z plane. (b) A magnetic field, $\mathbf{H}$ is applied along the z-axis in the +z direction. Due to the $\mathbf{H}$ field, magnetic monopoles curve upward and anti-monopoles curve downward in the x, z plane.

The track x, y data for *bobby pins*, the example track, was digitized using the ImageJ package and fit to Eq. (2), of the generalized quadratic equations

$$y = \frac{\sqrt{-b + (b^2 - 4a(c - x))}}{2/a} \tag{2}$$

$$y = \frac{\sqrt{-b + (b^2 - 4a(c - x))}}{2/a} + \mathrm{o} \tag{3}$$

$$y = \frac{\sqrt{-b + (b^2 - 4a(c - x)))}}{2/a}, \quad \text{where}$$

$$y = \frac{x}{y} + \mathrm{o}, \tag{4}$$

which all describe parabolas, where a, b and c are coefficients and o is an offset. The fit target was the lowest sum of absolute square error. Lower numbers for both R-squared and RMSE means a better fit. The mean goodness-of-fit of the generalized quadratic equations to the plotted data is $\overline{R}^2 = 0.998$ [1].

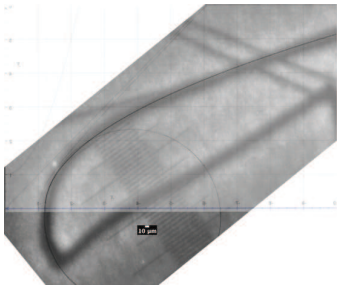

Figure 28. Track 4. *Bobby pins* was visually fit in this image to the parabola $y = x^2$ and a circle for comparison.

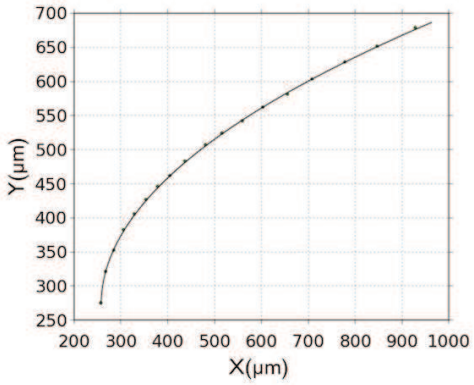

Figure 29. Track 4. *Bobby pins* fit to general quadratic equation (2).

Overall, this sample of tracks (and others in the study) show a nearly perfect fit to quadratic equations and therefore to parabolic trajectories. Parabolic curvature in the x, z plane with an applied magnetic field on the z-axis in searches for monopoles [25,26] is considered a strong signature for a magnetically charged particle [25, 27–29] since *parabolic curvature is unique*. But parabolic curvature is observed in the x, y plane with an applied magnetic field on the z-axis. A solution to this problem is shown in Section 7.

5.2. Momentum estimates

Momentum was estimated using 18 curved segments in two-tailed tracks using the following criteria:

(1) must be a two-tailed track with a vertex,
(2) one tail must have smooth curvature,
(3) must have a twin track,
(4) magnetic field strength is known.

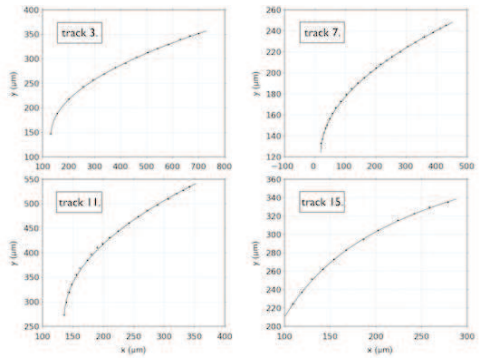

Figure 30. Tracks 3, 7, 11 and 15 curve fits to general quadratic equations (2)–(4) showing graphical fits to parabolas.

The computation below uses the kinetic energy, E_{k} computed with the general energy loss model in Section 6.1. For a magnetically charged particle, the analogous formula for parabolic electrostatic deflection for a particle traveling in the x direction in the x, y plane is used where

$$y = \frac{e|\mathcal{E}|x^2}{2mv_x^2}. \tag{5}$$

Substituting B, the magnetic field strength for $\mathcal{E}$, the electric field strength and $g = g_{\mathrm{D}} = (137/2)e$ (Dirac case) or $g = -e$ (Recami-Mignani [30] case), magnetic charge for e, electric charge, becomes

$$y = \frac{g|B|x^2}{2mv_x^2}, \tag{6}$$

where $mv = p$ and $v/c = \beta = pc/E$ where E is energy, v the velocity and p is the momentum. In natural units (where $c = 1$) momentum is given by

$$p_i = \sqrt{\frac{g|B|x^2}{2y/E}} \tag{7}$$

where p_i is the ith computed momentum value using known values for x, y and E in Eq. (7). Average momentum, $\overline{p}$ is estimated using

$$\overline{p} = \frac{1}{n}\sum_{i=1}^{n} p_i \tag{8}$$

6. Energy Loss

The energy loss in the emulsion is computed based on the number of developed (or bleached) AgBr grains in a cylindrical track [11]. The tracks are observed in the gelatin, between the gelatin/air interface and the gelatin/plastic base interface. This can be verified by viewing track sharp focus at different depths between these interfaces using a microscope at 100× (or more) magnification. There is no concrete idea of the mechanism of track formation due to either radiative or ionization mechanisms, so a general model of energy loss based on deposited energy will be used.

6.1. Generalized model

Katz and Kobetich [31] show that 63% of grains in an emulsion are developed (or bleached) when the energy is between 230 and 400 eV/grain. For our purposes here, it is estimated that ∼90% of grains would be developed at a minimum of ∼600 eV/grain producing a saturated track after our uniform pre-exposure energy of ∼150 eV/grain.

In this model a track exposure of 600 eV/grain creates a saturated track. This is a preliminary simplified model of energy level per grain where it is assumed that energy loss is the same at all values of β and energy loss is based on ionization. Adjusting the value for eV/grain can accommodate other energy loss models such as radiative models. This can be also be improved in the future to better reflect known energy losses at different values of β and by including various energy loss levels.

Our example track is 1.33 cm and comprised of [1]

$$(1.15 \times 10^8 \text{ grains})(600 \text{ eV/grain}) = 6.9 \times 10^{10} \text{ eV}, \tag{9}$$

Table 1. Linear stopping power based on the general model, measured values of number of grains, N_{grains} and track length, L for sample tracks.

Track	cS (GeV/cm)	N_{grains}	L (cm)
"69 mm" fig:69mm	1051.0	1.2×10^{10}	6.90
"67 mm"	467.1	5.2×10^{9}	6.74
"hyper"	168.2	8.7×10^{8}	3.10
"short rev"	116.8	1.2×10^{8}	0.61
"rev caterpillar"	81.1	1.6×10^{7}	0.12
"bobby pins"	51.9	1.2×10^{8}	1.33
"curve swarm"	29.2	1.7×10^{7}	0.35
"birds"	13.0	5.2×10^{6}	0.24

and in general energy loss per unit path or linear stopping power is

$$\begin{aligned} S_{\text{linear}} &= \frac{\mathrm{d}E}{\mathrm{d}x} = \frac{6.9 \times 10^{10}\ \text{eV}}{1.33\ \text{cm}} = 5.187 \times 10^{10}\ \text{eV/cm} \\ &= 51.87\ \text{GeV/cm}, \end{aligned} \tag{10}$$

and with density, ρ of AgBr photographic emulsions at 3.82 g/cm^3, mass stopping power is

$$\begin{aligned} S_{\text{mass}} &= \frac{\mathrm{d}E/\mathrm{d}x}{\rho} = \frac{5.187 \times 10^{10}\ \text{eV/cm}}{3.82\ \text{g/cm}^3} \\ &= 1.36 \times 10^{10}\ \text{eV}\,\text{cm}^2/\text{g} \\ &= 13.6\ \text{GeV}\,\text{cm}^2/\text{g}. \end{aligned} \tag{11}$$

7. Superluminal Lorentz Transformation

The transformation from bradyonic (slower-than-light) inertial frames to tachyonic inertial frames allows us to shift between timelike and spacelike objects. The superluminal Lorentz transformation (SLT) [30,33,34] extends the special theory of relativity to superluminal frames and observers. Most importantly for our purposes, the SLT makes possible the interpretation of experimental data where superluminal objects are observed in subluminal frames.

The SLT is required to make sense out of observations made of superluminal objects from frame f' in the subliminal laboratory frame f.

7.1. Energy–momentum

Measured values of kinetic energy and momentum for our 18 tracks plotted on a graph in Fig. 31 fall in the area for $v > c$ particles. Measured values for kinetic energy, E_{k} and momentum, p are compared with known particles, i.e. electrons, protons and photons on this graph. Values for the Recami–Mignani model are shown here. Values for the Dirac model are shown in [1].

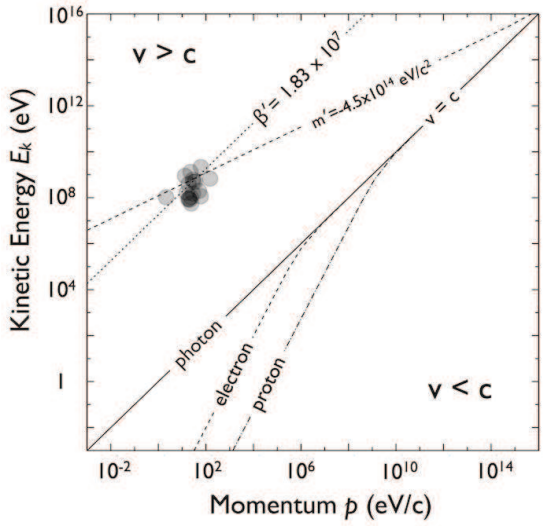

Figure 31. A Recami–Mignani tachyon monopole with monopole charge, $g = -e$ (in Gaussian units). Measured values for momentum and kinetic energy are clustered in the *faster-than-light* ($v > c$) area of the graph with a mass contour line computed with Eq. (17) intersecting the peak mass value of $|m| = 4.5 \times 10^5$ GeV/c^2. The velocity contour line intersects the SLT β value, $1/\overline{\beta} = \overline{\beta}'$ for our 18 tracks. Note also that as the SLT transforms $p' \rightleftarrows E_{\rm k}$, coordinate axes are reversed above $v = c$. Graph concept after Fraundorf [35].

Mass of particle tracks is estimated by inserting measured values of kinetic energy, $E_{\rm k}$ and momentum, p into the relativistic energy–momentum equation

$$c^2p^2 = E_{\rm k}^2 + 2E_{\rm k}mc^2 \tag{12}$$

solving for mass,

$$m = \frac{p^2c^2 - E_{\rm k}^2}{2E_{\rm k}c^2} \tag{13}$$

or, in natural units with $c = 1$

$$m = \frac{p^2 - E_{\rm k}^2}{2E_{\rm k}}. \tag{14}$$

This computation yields an average mass value of $|\overline{m}| = 227.58$ MeV/c^2 at an average velocity of $\overline{\beta} = 1.34\times10^{-6}$. The mass and velocity contours for the standard computation using Eq.(14) intersect in the wrong half (the $v < c$ half) of the graph and $E_{\rm k}$ is off by twelve orders of magnitude. The lack of agreement between the raw plotted data and mass computed using Eq. (14) inclines us to reject this particle mass result.

To estimate a *tachyon mass* the observables $E_{\rm k}$ and p need to be transformed from frame f to frame f' using an SLT of Eq. (14)

$$m' = -\frac{p'^2 - E_{\rm k}'^2}{2E_{\rm k}'}, \tag{15}$$

where the values of E and p are interchanged like $E'_{\rm k} = p$ and $p' = E_{\rm k}$ and the sign changes [1]. $\beta = p/E$ is transformed with an SLT as $\beta' = 1/\beta$.

Mass contours are found using

$$p = \sqrt{E_{\rm k}^2 + 2E_{\rm k}m} \tag{16}$$

for $v < c$ given values of m and $E_{\rm k}$, and

$$p' = \sqrt{E_{\rm k}'^2 + 2E'_{\rm k}m'} \tag{17}$$

for $v > c$, given values of m' and E'_k.

Using Eq. (15) for Recami–Mignani tachyon monopoles gives $|\overline{m}'| = 7.29 \times 10^6$ GeV/c^2 and $\overline{\beta}' = 1.83 \times 10^7$. This mass estimate should be taken as a lower limit of particle mass as (we assume) less than the actual particle kinetic energy is deposited in the track.

Figure 31 features contour lines for both velocity and mass. While the "raw" $E_{\rm k}$ and p values are directly plotted on the graph, the contour lines β' and m' on the upper $v > c$ half of the graph were found using a superluminal Lorentz transformation. Since the SLT is a special transformation *only applied in the case of superluminal particles*, this corroborates the identification of this particle as superluminal.

The estimate of particle mass was made based on a mass contour line intersecting with the cluster of data points. The peak mass value of $|m'| = 4.5 \times 10^5$ GeV/c^2 for Recami–Mignani tachyon monopoles (see Ref. [1] was inserted into Eq. (17) for a range of energy and momentum values and plotted as the dashed mass contour line intersecting the cluster of points in Fig. 31. This agreement between the raw plotted $E_{\rm k}$ and p values, the SLT peak mass, m' computed with Eq. (15), and velocity, $\beta' = 1/\beta$ intersecting as contours, constitutes an independent check of the data.

The measured kinetic energy value depends on the estimate of energy loss per grain that was used in the computation. In the general model computation, a 600 eV/grain base energy was used with an additional assumption of 150 eV/grain for the supplemental pre-exposure energy. If a base energy of 50 eV/grain is used, putting the total energy per grain at 200 eV, which is below the minimum value (for 63% of grains to be developed) of 230 eV/grain [31], the minimum kinetic energy value is still well above 10^4 eV and still above the $v = c$ contour line.

Measured average momentum depends on Eq. (7), the measured kinetic energy and the computed value of the magnetic field. The average momentum values on the plot in Fig. 31 are over three orders of magnitude (eV/c) from the $v = c$ line in the case of the Recami–Mignani tachyon monopole [36].[b]

7.2. Electromagnetic field

Parabolic curvature in magnetic fields as shown in section section:parabolic-curvature is expected of magnetic monopoles, however the curvature is seen (paradoxically) in the x, y plane instead of the x, z plane as expected. The orientation of the magnetic field in our experiments (Fig. 8) is clearly perpendicular to the x, y plane.

[b] Assuming circular curvature in the Dirac model we found $\overline{p} \simeq 519$ eV/c.

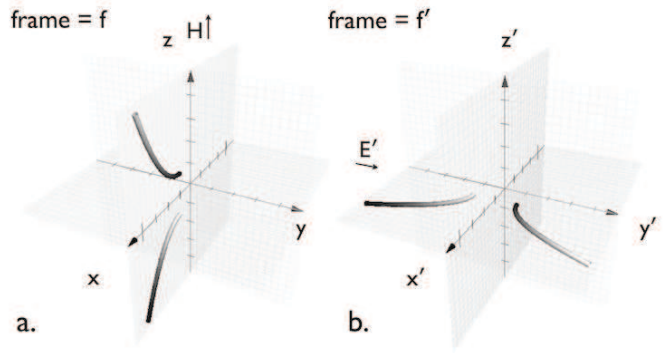

Figure 32. (a) Frame f where a magnetic field applied parallel to the z-axis is expected to cause parabolic curvature for magnetically charged bradyons in the x, z plane. (b) For *tachyons*, parabolic curvature occurs for electrically charged tachyons in the frame f' in the x', y' plane. For observables connected with electromagnetic fields, frame f' is related to frame f by a superluminal Lorentz transformation where $\mathbf{H}_z = \mathbf{E}'_y$.

Recami and Mignani show [32,33] the electrically charged tachyon in the bradyonic frame as possessing magnetic charge $g = -e$ (in Gaussian units) (as opposed to the "standard" $g = g_{\mathrm{D}} = e(137/2)$). This theory is symmetric between subluminal and superluminal frames with $v = c$ the partition between frames.

Superluminal particles in f' with electric charge behave as magnetic monopoles in our subluminal frame f, but to make sense of the observables in f we need to transform as $f \xrightarrow{\text{SLT}} f'$ [30,33]. Since the velocity u, $(0 < u < c)$ of frame f differs from the velocity $U = c^2/u$, $(U > c)$ of frame f' as $U \to \pm\infty$, we use the *transcendent SLT* [30,33,37], recami.transcendent,recami.classical,recami.applications which rotates coordinate axes by either 90° or 270° as well as swapping $\mathbf{E}$ and $\mathbf{H}$.

By using this transformation we rectify the paradox of parabolic particle tracks observed in the plane perpendicular to the applied magnetic field. Thus it is possible to interpret our parabolic tracks in photographic emulsions as due to electrically charged tachyons. Measurement of the parabolic curvature of these tracks also importantly allowed us in Section 5.1 to estimate the particle momentum using Eq. (7).

7.3. Tachyon shape

Assuming that the tachyon has a spherical shape in its restframe, f', an SLT is applied to determine how the tachyon would appear to a subluminal observer in frame f. After application of the SLT, the tachyon shape becomes a *hyperbolic annulus* [33,38]. The intersection of this shape, orthogonal to the particle's motion is an annulus or a ring (or dot) comprised of the area between two concentric circles [39].[c]

This agrees with certain perpendicularly incident tracks seen in Fig. 9. This also coincides directly with some of the unusual track shapes (Figs. 19 and 35 shown in [13] studies and is of interest to replicate. Compare also with periodic circles in Fig. 7.

The intersection of the double hyperbolic annulus with a plane parallel to the tachyon motion appears as an x-shaped object as in Fig. 36a. This corresponds to a track in the plane of the emulsion. It is possible to simulate periodic tracks such as in Section 3.5 by constructing repeating conic sections as in Fig. 36b.

[c]See also Figs. 3, 5 and 6 of Ref. [38].

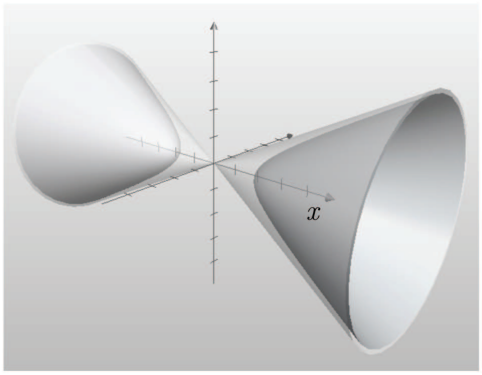

Figure 33. Shape of tachyon (between conic and hyperbolic surfaces) with motion in x direction after an SLT as a subluminal observer in frame f would see it.

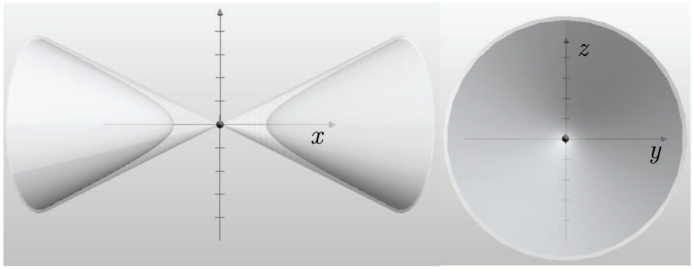

Figure 34. Top and end views of tachyon shape.

Figure 35. Ring track of Matsumoto

The horizontally incident tracks in this concept appear to be akin to a collective excitation and might be physically modeled by a series of tachyon creations and annihilations arising from *vacuum fluctuations* propogating in space [33]. See also Fig. 16 of Ref. [1] and Fig. 35 of [33].

7.4. Summary

We found values of E_k and p indicating superluminal particles. To find m and β consistent with the observables E_k and p, *an SLT was required*. Curvature of our sample tracks was found to be parabolic, indicating magnetic monopoles, but the plane of detection was perpendicular rather than parallel to the applied magnetic field. An SLT applied to the coordinate system shifts the **H** and **E** fields and rectifies the explanation of the particle as a tachyon monopole. Extending this analysis to certain particle tracks we find a possibility that tachyon shape, transformed using an SLT, may correspond with certain types of particle tracks.

8. Discussion

Analyzing the exposed area of a track in the emulsion Urutskoev and co-workers [2] estimated kinetic energy at $E \sim$700 MeV. This is one order of magnitude lower than the average non-ζ-corrected energy value for our 18 tracks of $E \simeq 1.7$ GeV, but much lower when compared with our longer (and thicker) tracks. Other tracks in Urutskoev and co-workers [2] and tracks in the other photographic studies [4–7,10,11] if examined for deposited energy (using ζ-correction) should all correspond within our limits.

Adamenko and Vysotskii [8,9] estimated an upper limit of kinetic energy at $E \sim -10^6$ GeV and particle mass at $\approx 10^{-23}$g ($\approx$ 560 GeV). Our peak mass values presented above fall above the 560 GeV value by two orders of magnitude. Our higest non-ζ-corrected energy values come in at 7.3×10^3 GeV, falling within the range below the upper limit of $E \sim -10^6$ GeV. Ivoilov [4] suggests that the particles may correspond to neutrinos of zero mass, which are monopoles [17] with a maximum value of $\sim$ 1 MeV. Our kinetic energy values are much greater than this and there is no agreement between our data and the Ivoilov energy data.

8.1. Further considerations

In the Recami–Mignani theory, the tachyon may be observed as a monopole in the ordinary subluminal laboratory frame. "Standard" monopole mass is estimated to be either on the order of the unification mass ($\approx 4\times10^{15}$ GeV)groom or, assuming the monopole has a radius equal to the classical electron radius, $m \approx 2.4$ GeV/c^2. Certain magnetic monopole searches have concentrated in the low to intermediate mass region [41] of 10^3 GeV/c^2 $< m_M <$ 10^{12} GeV/c^2. Our lower limit peak mass values of $|m| = 5.4 \times 10^4$ GeV/c^2 and $|m| = 4.5 \times 10^5$ GeV/c^2 are consistent with that range.

Figure 36. (a) Intersection of tachyon with plane parallel to particle motion on x axis. (b) Simulation of "M" components of track with periodic structure using conic sections. (c) Track from Fig. 4 exhibiting periodic structure.

The Recami–Mignani model however assumes a monopole charge of $g = -e$ (in Gaussian units) rather than the standard Dirac charge of $g = g_{\mathrm{D}} = (137/2)e$. For our purposes the difference in charge simply shifts the raw momentum and mass values lower by about an order of magnitude. Tachyons traveling as identical particles should behave as like charges that attract the same way as ordinary wires carrying electric current [38]. These tachyons could coalesce in bundles and split apart in applied electromagnetic fields.

In the model of Fried [42] where tachyons contribute to dark matter, tachyons are expected with masses on the order of 10^6–10^8 GeV. These tachyons are also expected to travel together over galactic distances in "lines" and "swarms." Our lower limit mass estimate is in agreement with these values. Both of the above theoretical considerations fit with the observation of bundles and splitting shown in Section 3.10.

9. Conclusion

The analysis presented here suggests the detection of Recami–Mignani tachyon monopoles with a lower limit of $|m| \sim 4.5 \times 10^5$GeV/c^2 (or $|m| \sim 5.4 \times 10^6$GeV/c^2 in the case of Dirac tachyon monopoles) that can travel in bundles of "identical" particles with regular periodic trajectories and various modes, dependent on energy level. At lower energies, particles may go into random motion. Correlation of pairs and groups of these particles is observed frequently.

In Section 6 measured energy and momentum values for our sample tracks indicate superluminal particles. This result is supported by the requirement to transform the data using an SLT to yield consistent mass and velocity values. In Section 5 parabolic curvature is observed in an applied magnetic field as would be expected for a magnetic monopole, except that the parabolic curvature is in the x, y rather than the x, z plane. Parabolic curvature in the x, y plane *perpendicular* to an applied magnetic field suggests the detection of a magnetic monopole in our local frame, which as shown in Section 7 is how an electrically charged tachyon in a superluminal frame appears in the local frame.

Using tachyon shape derived using the SLT shows possible agreement with ring and periodic structure images which may be further associated with collective excitations or vacuum fluctuations. Further study of the image formation, energy deposition, curvature in magnetic fields, bundling, splitting, vertexes and correlation of these particles is indicated to get a clear picture of their properties.

Acknowledgments

The author thanks Leonid Urutskoev, Moses Fayngold, Matej Pavšič, Erasmo Recami, Anri Ruhkadze, Mark Davidson, Irina Savvatimova and Nikolay Ivoilov for helpful comments and kind interest.

References

[1] K.A. Fredericks, *Eng. Phys.* **6** (2013) 15; Eprint online (2013).
[2] L.I. Urutskoev, V.I. Liksonov and V.G. Tsinoev, *Ann. Fond. L. de Broglie* **27** (2002) 701; ArXiv Physics e-prints (2001), arXiv:physics/0101089.
[3] L.I. Urutskoev, *Ann. Fond. L. de Broglie* **29** (2004) 1149.
[4] N.G. Ivoilov, *Ann. Fond. L. de Broglie* **31** (2006) 115.
[5] N.G. Ivoilov and L.I. Urutskoev, *Ann. Fond. L. de Broglie* **29** (2004) 1177.
[6] D. Priem et al., *Ann. Fond. L. de Broglie* **34** (2009) 103.
[7] G. Bardout, G. Lochak and D. Fargueb, *Ann. Fond. L. de Broglie* **32** (2007) 551.
[8] V. Adamenko and V.I. Vysotskii, in *Proc. of the 14th Int. Conf. on Condensed Matter Nuclear Science and the 14th Int. Conf. on Cold Fusion (ICCF-14)*, 10–15 August 2008, Washington DC, D.J. Nagel and M.E. Melich (Eds.), New Energy Foundation Inc., 2008, p. 484.

[9] S.V. Adamenko and V.I. Vysotskii, A*nn. Fond. L. de Broglie* **33** (2008) 13.
[10] B. Rodionov and I. Savvatimova, in *12th Condensed Matter Nuclear Science*, Vol. 12 A. Takahashi, K.- I. Ota and Y. Iwamura (Eds.). 2006, pp. 421–429.
[11] I. Savvatimova and J. Dash, in *The 9th Int. Conf. on Cold Fusion, Condensed Matter Nuclear Science*, 2002. Tsinghua Univ., Beijing, China, Z.Z. Li (Eds.), Tsinghua Univ. Press, 2002.
[12] T. Matsumoto, *Fusion Technol.* **18** (1990) 356.
[13] T. Matsumoto, *Bulletin of the Faculty of Engineering,* Hokkaido Univ. No. 175 (1995), p. 73.
[14] E. Storms, *21st Century Sci. ang Technol. Winter*, 76 (2000).
[15] E. Storms, Student's Guide to Cold Fusion, revised (2012), lenr-canr.org.
[16] E. Storms, What is now known about cold fusion? (Ad- dendum to the Student's Guide) (2011), lenr-canr.org.
[17] G. Lochak, *Z. Naturforsch.* **A62** (2007) 231, arXiv:0801.2752 [quant-ph].
[18] D. Priem et al., *Ann. Fond. L. de Broglie* **33** (2008) 129.
[19] G. Lochak, personal communication.
[20] G. Lochak, Traces of monopoles observed in laboratory, (2013) lochak.com website.
[21] G. Lochak and L. Urutskoev, in Condensed Matter and Nuclear Science, *Proc. of the 11th Int. Conf. on Cold Fusion*, 31 October–5 November, Marseille, France, 2004, J. Biberian (Ed.), World Scientific, London, 2006, p. 421.
[22] [22] R. Katz and D.R. Parnell, *Phys. Rev.* **116** (1959) 236.
[23] T.E. Furtak and R. Katz, *Radiat. Effects* **11** (1971) 195; Eprint online (1971).
[24] C.F. Powell, *The Study of Elementary Particles by the Photographic Method*, Pergamon Press, London, 1959.
[25] W. Braunschweig et al., *Z. Phys. C* **38** (1988) 543, 10.1007/BF01624358.
[26] T. Gentile et al., *Phys. Rev. D* **35** (1987) 1081.
[27] A. Abulencia et al. (CDF Collaboration), *Phys. Rev. Lett.* **96** (2006) 201801.
[28] CDF (The CDF Collaboration), A direct search for dirac magnetic monopoles, (2004), the CDF Collaboration 2004, CDF note 7183.
[29] A. Aktas et al. (H1 Collaboration), *Eur. Phys. J.* **C41** (2005) 133, arXiv:hep-ex/0501039 [hep-ex].
[30] E. Recami and R. Mignani, *Nuovo Cimento* **4** (1974) 209.
[31] R. Katz and E.J. Kobetich, *Phys. Rev*. **186** (1969) 344.
[32] J. Beringer et al. (Particle Data Group), *Phys. Rev. D* **86** (2012) 010001.
[33] E. Recami, *Nuovo Cimento* **9** (1986) 1, 10.1007/BF02724327.
[34] L. Parker, *Phys. Rev.* **188** (1969) 2287.
[35] P. Fraundorf, A conservation-law view of everyday motion (2007), Department of Physics and Astronomy and Center for NanoScience at the University of Missouri in Saint Louis.
[36] Assuming circular curvature in the Dirac model we found $p \simeq 519$ eV/c.
[37] R. Mignani and E. Recami, *Il Nuovo Cimento A* **14** (1973) 169.
[38] A. Barut, G. Maccarrone and E. Recami, *Nuovo Cimento A* **71** (1982) 509, 10.1007/BF02770989.
[39] See also Figs. 3, 5 and 6 of Ref. [38].
[40] D.E. Groom, *Phys. Reports* **140** (1986) 323.
[41] G. Giacomelli, S. Manzoor, E. Medinaceli and L. Patrizii, *J. Phys. Conf. Ser.* **116** (2008) 012005, arXiv:hep- ex/0702050 [HEP-EX].
[42] H. Fried and Y. Gabellini (2007), arXiv:0709.0414 [hepth].